Proposal to Jefferson Lab PAC 38

PREX-II: PRECISION PARITY-VIOLATING MEASUREMENT OF THE NEUTRON SKIN OF LEAD

Spokespersons: K. Paschke, K. Kumar R. Michaels, P.A.Souder, G.M. Urciuoli

P.A. Souder, R. Holmes, Chun-Min Jen, L. Zana, Z. Ahmed, A. Rakhman
Syracuse University

E. Cisbani, S. Frullani, F. Garibaldi, F. Meddi, G.M. Urciuoli, M. Capogni
INFN / Rome

K. Allada, A. Camsonne, A. Deur, J.P. Chen, O. Hansen, D. Higinbotham,
J. Gomez, J. LeRose, R. Michaels, S. Nanda, B. Sawatzky, B. Wojtsekhowski, J. Zhang
Thomas Jefferson National Accelerator Facility

K. Kumar, S. Riordan, L. Mercado, J. Wexler, S. Johnston, J. Mammei
University of Massachusetts

A. D'Angelo, C. Schaerf, I. Zonta
INFN / Rome Tor Vergata

R. De Leo, L Lagamba
INFN/Bari

E. Bellini, A. Giusa, F. Mammoliti, G. Russo, L. Sperduto, C. Sutera
INFN/Catania

M. Aghasyan, E. De Sanctis, D. Hasch, V. Lucherini, M. Mirazita, S. A. Pereia, P. Rossi
INFN/Frascati

K.A. Aniol, D. J. Margaziotis
California State University, Los Angeles

T. Averett, D. Armstrong, W. Deconinck, J.F. Dowd
College of William and Mary, Virginia

C.J. Horowitz, S. Ban
Indiana University

R. Wilson
Harvard University

G.D. Cates, J. Liu, K. Paschke, R. Silwal, K. Saenboonruang
M. Dalton, D. Wang, Z. Zhao, X. Zheng
University of Virginia

P. Markowitz, P. Khetarpal
Florida International University

S. Kowalski, J.F. Rajotte, V. Sulkosky
Massachusetts Institute of Technology

O. Glamazdin, R.Pomatsalyuk
National Science Center Kharkov Institute of Physics and Technology

R. Perrino
INFN/Lecce

M. Battaglieri, A. Celentano, R. De Vita, M. Osipenko, M. Ripani, M. Taiuti
INFN/Genova

2

L. Barion, G. Ciullo, M. Contalbrigo, P.F. Dalpiaz, P. Lenisa, L.L. Pappalardo
INFN/Ferrara

J. Roche, P. King
Ohio University

D. McNulty
Idaho State University

R. Gilman, L. El Fassi
Rutgers University

P. Decowski
Smith College

This is a Hall A Collaboration Proposal

The proposal and related information is at
http://hallaweb.jlab.org/parity/prex

ABSTRACT

This is a follow-up measurement to PREX-I which ran in 2010 and demonstrated successful control of systematic errors and overcame many technical challenges, but which ran into difficulties with radiation and the vacuum system that reduced the running efficiency. PREX measures the parity-violating electroweak asymmetry in the elastic scattering of polarized electrons from ^{208}Pb at an energy of 1.0 GeV and a scattering angle of 5°. Since the Z^0 boson couples mainly to neutrons, this asymmetry provides a clean measurement of R_N, the RMS radius of neutrons in a heavy nucleus. PREX-I was statistics limited, yet already established the existence of the neutron skin at the 95% confidence level. PREX-II is designed to achieve the originally proposed experimental precision in R_N of ± 1 %. In addition to being a fundamental test of nuclear theory, a precise measurement of R_N pins down the density dependence of the symmetry energy of neutron rich nuclear matter which has impacts on neutron star structure, heavy ion collisions, and atomic parity violation experiments. We are requesting 35 days of polarized beam running in Hall A at 925 to 1000 MeV using the 5° degree septum magnets. This includes 5 days of commissioning and 5 days of overhead for Møller Polarimetry and auxiliary measurements.

PREX-II ^{208}Pb Parity

PREX-I ran from March 19 to June 20, 2010. It achieved the systematic error goals (2%) and was a major accomplishment as a first measurement of its kind with many milestones successfully achieved; however, because of various problems the experiment took only ∼15% of the planned statistics. This proposal is a followup measurement with anticipated improvements to take data at a rate equivalent to the original proposal estimates.

This proposal and related materials are all available on the experiment's web site: http://hallaweb.jlab.org/parity/prex

I   INTRODUCTION

Nuclear charge densities have been accurately measured with electron scattering and have become our picture of the atomic nucleus, see for example ref. [1]. These measurements have had an enormous impact. Unfortunately, bulk neutron densities are not directly probed in electron scattering because the neutron is uncharged. In contrast, our knowledge of neutron densities comes primarily from hadron scattering experiments involving for example pions [2], protons [3–5], or antiprotons [6,7]. However, the interpretation of hadron scattering experiments is model dependent because of uncertainties in the strong interactions. Particular probes may have additional uncertainties. For example antiprotons may only probe the large radius tail of the neutron density, because of strong absorption. Therefore neutron densities, deduced from hadron scattering, could have significant strong interaction uncertainties.

Parity violating electron scattering provides a model independent probe of neutron densities that is free from most strong interaction uncertainties. This is because the weak charge of a neutron is much larger than that of a proton [8]. Therefore the Z^0 boson, that carries the weak force, couples primarily to neutrons. In Born approximation, the parity violating asymmetry A_{pv}, the fractional difference in cross sections for positive and negative helicity electrons, is proportional to the weak form factor. This is closely related to the Fourier transform of the neutron density. Therefore the neutron density can be extracted from an electro-weak measurement [8]. However, the Born approximation is not valid for a heavy nucleus and coulomb distortion effects must be included. These have been accurately calculated [9]. Many details of a practical parity violating experiment to measure neutron densities have

been discussed in a long paper [10].

To illustrate the sensitivity to R_N we write the asymmetry in Born approximation

$$A_{pv} = \frac{G_F Q^2}{4\pi\alpha\sqrt{2}} \left[1 - 4\sin^2\theta_W - \frac{F_n(Q^2)}{F_p(Q^2)} \right] \qquad (1)$$

where G_F is the Fermi constant, $\alpha = \frac{1}{137}$ is the fine structure constant, θ_W is the Weinberg angle, and $F_n(Q^2)$ and $F_p(Q^2)$ are the neutron and proton form factor of the nucleus.

The Lead Radius Experiment (PREX) measures the parity violating asymmetry A_{pv} for 1.063 GeV electrons scattering from ^{208}Pb at five degrees. This measurement should be sensitive to the neutron r.m.s radius of ^{208}Pb to 1% (± 0.05 fm).

The doubly magic nucleus ^{208}Pb has 44 more neutrons than protons, and some of these extra neutrons are expected to be found in the surface where they form a neutron rich skin. The thickness of this skin is sensitive to nuclear dynamics and provides fundamental nuclear structure information. There may be a useful analogy with cold atoms in laboratory traps where similar "spin skins" have been observed for partially polarized systems [11] [12].

The neutron radius of ^{208}Pb, R_N, has important implications for astrophysics. There is a strong correlation between R_N and the pressure of neutron matter P at densities near 0.1 fm^{-3} (about 2/3 of nuclear density) [13]. A larger P will push neutrons out against surface tension and increase R_N. Therefore measuring R_N constrains the equation of state (EOS) — pressure as a function of density — of neutron matter. The equation of state is very important in astrophysics to determine the structure of neutron stars.

Recently Hebeler et al. [14] used chiral perturbation theory to calculate the EOS of neutron matter including important contributions from very interesting three neutron forces. We have some information on isospin 1/2 three nucleon forces from mass 3 nuclei (^{3}He, ^{3}H) and proton-deuteron scattering. However, our experimental information on three neutron forces is limited. From their EOS, they predict $R_N - R_P = 0.17 \pm 0.03$ fm. Here R_P is the known proton radius of ^{208}Pb. Monte Carlo calculations by Carlson et al. also find sensitivity to three neutron forces [15]. Therefore, measuring R_N provides an important check of fundamental neutron matter calculations, and constrains three neutron forces.

The correlation between R_N and the radius of a neutron star r_{NS} is also very interesting [16]. In general, a larger R_N implies a stiffer EOS, with a larger

6

pressure, that will also suggest r_{NS} is larger. Note that this correlation is between objects that differ in size by 18 orders of magnitude from $R_N \approx 5.5$ fm to $r_{NS} \approx 10$ km. Recently there has been great progress in deducing r_{NS} from X-ray observations. Ozel et al. find r_{NS} is very small, near 10 km from observations of X-ray bursts [17], while Steiner et al. [18] conclude that r_{NS} is near 12 km and predict that $R_N - R_P = 0.15 \pm 0.02$ fm. The high density EOS implied by Ozel et al. [19] is soft, suggesting a transition to an exotic phase of QCD. In contrast, the Steiner et al. EOS is stiffer, leaving little room for softening due to a phase transition. These results can be tested with a measurement of R_N.

The EOS of neutron matter is closely related to the symmetry energy S. This describes how the energy of nuclear matter rises as one goes away from equal numbers of neutrons and protons. There is a strong correlation between R_N and the density dependence of the symmetry energy $dS/d\rho$, with ρ the baryon density. The symmetry energy can be probed in heavy ion collisions [20]. For example, $dS/d\rho$ has been extracted from isospin diffusion data [21] using a transport model.

The symmetry energy S helps determine the composition of a neutron star. A large S, at high density, implies a large proton fraction Y_p that will allow the direct URCA process of rapid neutrino cooling. If $R_N - R_P$ is large, it is likely that massive neutron stars will cool quickly by direct URCA [22]. In addition, the transition density from solid neutron star crust to the liquid interior is strongly correlated with $R_N - R_P$ [23].

Finally, atomic parity violation (APV) is sensitive to R_N [24], [25], [10]. A future low energy test of the standard model may involve the combination of a precise APV experiment along with PV electron scattering to constrain R_N. Alternatively, measuring APV for a range of isotopes can provide information on neutron densities [26].

II   PHYSICS RESULTS OF PREX-I

The PREX-I results were shown at the April 2011 APS conference and a physics letter (PRL) is in preparation for publication. The experiment ran in Spring 2010 at 1.063 GeV energy with a new warm-temperature septum magnet at a central scattering angle of 5° with 50-70μA beam current. The sign of the laser circular polarization determined the electron helicity, which was selected at 120 Hz. To avoid noise from the 60 Hz line power cycle, the asymmetry was measured in "quadruplets": 4 helicity states in the patterns RLLR or LRRL, with the polarity of each pattern determined pseudo-randomly. The integrated response of each detector PMT and beam monitor was digitized by

7

a custom, low-noise 18-bit ADC and recorded for each helicity period. Periods of instability in the electron beam trajectory and intensity were removed during offline analysis. No helicity-dependent cuts were applied. The final data sample consisted of 1.94×10^7 quadruplets.

The measured asymmetry was corrected for a false asymmetry A_{Beam} induced by helicity-correlated changes in the beam trajectory Δx_i and energy A_E, $A_{beam} = \Sigma_i c_i \Delta x_i$. The factors c_i were measured several times each hour from calibration data in which the beam was modulated by using steering coils and an accelerating cavity. The largest of the c_i was on the order of 50 ppb/nm. This correction removed noise in the measured asymmetry due to beam jitter at the 8.3 ms time scale of about 20 μm in position and 2 ppm in energy. The noise in the resulting $A_{corr} = A_{raw} - A_{beam}$ was about 200 (171)ppm per quadruplet, for running with a beam current of 50 (70) μA. The noise is dominated by counting statistics, corresponding to a rate of about 1GHz at 70μA, consistent with rate estimates from low current calibration runs. See fig 1 for the asymmetry distribution observed at 70μA, where we ran for the last four days of the run. The distribution is a clean Gaussian with a width of 171 ppm.

Due to beam damage, the thickness of the lead foil targets became non-uniform in the area covered by the beam raster after a few days of running. The variation of the average target thickness between helicity states, caused by incomplete raster cycles and the non-uniform target, became a significant source of noise. This excess noise was eliminated by locking the raster pattern repetition frequency to the helicity-reversal frequency.

A half-wave ($\lambda/2$) plate was periodically inserted into the laser optical path which passively reversed the sign of the electron beam polarization. Roughly equal statistics were thus accumulated with opposite signs for the measured asymmetry, which suppressed many systematic effects. An independent method of helicity reversal was provided by a pair of Wien spin-filters separated by a solenoid near the injector was installed. By reversing the direction of the field in the solenoid, the beam helicity could be reversed. However, the electron beam optics, which depends on the square of the magnetic field, was unchanged. This additional spin flip provides a powerful check for systematic errors. The ($\lambda/2$) reversal was done about every 12 hours and the solenoid reversal was performed every few days. Under the reversals, the absolute values of A_{corr} are consistent within statistical errors.

Averaged over all runs, the $A_{corr} = +593 \pm 51(\text{stat}) \pm 10(\text{syst})$ ppb. Since the differences in the position monitors and beam energy average the entire experiment were only 4 nm and 0.6 ppb, respectively, the average corrections due to systematic helicity-correlated differences in beam parameters were small.

The physics asymmetry A_{PV} is formed from A_{corr} by correcting for the beam polarization P_b, background fractions f_i with asymmetries A_i and finite kinematic acceptance K. The diamond cooling foil contributed $6.6 \pm 0.6\%$ of the measured signal, but because A_{PV} is similar for carbon and lead elastic scattering, the net correction was smaller, $1.6\pm0.5\%$. Contributions from inelastic states and re-scattered backgrounds were negligible. The acceptance correction K accounted for the non-linear dependence of the asymmetry with Q^2. A significant systematic error in $\langle Q^2 \rangle$ is in the determination of the absolute scale of the scattering angle θ_{lab}. A nuclear recoil technique with a dedicated calibration run using a water cell target was used to set a scale error on Q^2 of $< 0.2\%$. Nonlinearity in the PMT response was limited to 1% in bench-tests that mimicked running conditions.

Beam polarization was measured using an energy-weighted integrating measurement of the asymmetry in Compton backscattered photons, to be $P_b = 88.20 \pm 1.0\%$. The beam polarization was monitored continuously by the polarimeter over the run, and was stable within systematic errors. The Møller polarimeter, which was upgraded to use a superconducting magnet to saturate the ferromagnetic target foil, measured $P_b = 90.32 \pm 1.1\%$ beam polarization. These measurements were averaged to $P_b = 89.2\pm1.0\%$, where the uncertainty was taken to be the smallest included in the average.

With all corrections, $A_{PV} = 657 \pm 60(\text{stat}) \pm 13(\text{syst})$ ppb at $Q^2 = 0.00906 \, \text{GeV}/c$. This corresponds to a value for $R_n - R_p = 0.34 + 0.15 - 0.17$ fm; confirming the existence of an neutron radius excess with a 2σ statistical significance. The result is consistent with all of the models shown in fig 15 (refs [27–32]). We are proposing here to reduce the error by a factor of 3 in a future run to be able to discriminate between the models and make predictions relevant to neutron stars and parity violation in atoms.

III   TECHNICAL MILESTONES DURING PREX-I

A   Septum Magnet

The new room-temperature septum magnet worked well. However, a problem found after the experiment was that the septum magnet setting was slightly too low; we ran at 729A, but 775A would have been optimal. This reduced our rates by about a factor of two, reducing our figure-of-merit (FOM) by 16%. For this measurement, the FOM is the error in the neutron radius, which we minimize by maximizing the product $R \times A^2 \times \epsilon^2$ where R is the rate, A is the asymmetry, and ϵ the sensitivity of A to R_N, i.e. $\epsilon = dA/A$

for a 1% change in R_N. This FOM varies rapidly with angle because the lead form factor drops rapidly. Fig 2 (left) shows the angle distribution of the data compared to simulation, where the simulation was performed at the correct septum field integral. Analysis of the optics calibration data (sieve slits) confirmed this interpretation. The analysis reconstructs the entrance angle into the high-resolution spectrometers (HRS) by back-tracking through the HRS using known matrix elements. It was found that the bending by each septum was ∼5 mrad less than expected, hence we were losing 5 mrad (0.3°) in the small-angle side of the acceptance. An analysis of the septum current scans performed during the experiment shows we could have gotten the full acceptance at the correct Q^2 by running the septum at 775 A together with moving the PREX detector to one side by 2.5 cm in the focal plane, an easy adjustment. Based on this experience we have a much better plan to quickly adjust the setup at the start of PREX-II to obtain the optimum FOM and avoid this problem. An insertable "sieve slit" (a tungsten plate with an array of holes) is used to calibrate the reconstruction of angles relative to the central angle in the region upstream of the septum magnet. The procedure will be to perform a current scan on the septum magnet until the sieve slit pattern is aligned, which is equivalent to having the correct Q^2.

B Double Wien Filter

A new "double-Wien filter" has been fabricated and installed at the injector beamline in Jan 2010 by the Polarized Injector Group. This device allowed us to flip the helicity about once a week using an arrangement of solenoids that flip the helicity without changing the beam trajectory. The Qweak experiment is also benefiting from this new device.

Figure 3 shows the helicity-correlated position differences and charge asymmetries achieved during PREX-I. Two kinds of slow helicity-reversals (flips) are used: insertable halfwave plate (IHWP) and the Wien filter. Without any flips, position differences of order 10 to 20 nanometer (nm) are observed. The data points are plotted without any sign correction to illustrate these systematics. With all the flips, these systematics cancel at the 5 nm level, making our corrections small compared to the statistical error and the systematic error due to beam asymmetries negligible. An advantage of the Wien flip is demonstrated by the additional suppression of these "first order" effects. It is also well-known in the parity community that the Wien flips have the additional advantage of suppressing possible "higher order" effects, e.g. a helicity-correlated spot size.

C   Transverse Asymmetry Systematic

We were concerned about possible systematic errors resulting from the product of transverse polarization of the beam and vector analyzing power for transverse asymmetry in elastic e-^{208}Pb scattering. Two important findings during the run eliminated this problem. First, the transverse asymmetry was measured to be $+0.22 \pm 0.42$ ppm on our lead target, which makes it a non-problem for the experiment. (This is a preliminary result; a publication is being prepared.) Second, we were able to find a location in the HRS focal plane to place an auxiliary detector which is sufficiently sensitive to a transverse asymmetry, due to higher order terms in the HRS.

The transverse asymmetry for ^{12}C was also measured and found to be -6.5 ppm, which was about the expected size and qualitatively consistent with the measurements of ^{4}He performed by our collaboration in 2004.

D   Polarimetry

The Compton and Møller polarimeters made major advances allowing us to achieve a 1.2% accuracy in beam polarization during the run. Incremental improvements for PREX-II should allow us to achieve a 1% level with two independent polarimeters

1   Møller Polarimeter

Just prior to PREX-I the Møller polarimeter was upgraded as follows: 1) The "brute force" polarization of the target foil using a strong (3T) magnetic field, as has been done in Hall C [33]. Also the target has a smaller thickness and lower heating; 2) A segmented aperture detector to accommodate the higher rates; and 3) A new fast DAQ based on Flash ADCs to handle the higher rates with smaller deadtime and to provide more information about the events such as pileup. Table 1 shows the systematic errors achieved during PREX-I which totaled 1.1%.

Since PREX-I ran, the Møller polarimeter has been restored to it's previous low-field magnet setup because this didn't require cryogenic cooling and because it was sufficient for anticipated running during g2p/GEp in late 2011. Restoring the high-field setup for PREX-II will require an approximately 2 month installation effort involving on average two technicians ($\sim 25\%$ time) and two visiting scientists full-time. The cryo load is substantial, about 16

TABLE 1. Møller Polarimeter Systematic Errors

Iron Foil Polarization	0.25 %
Targets Discrepancy	0.5%
Target Saturation	0.3%
Analyzing Power	0.3%
Levchuk Effect	0.5%
Target Temperature	0.02%
Deadtime	0.3%
Background	0.3%
Other	0.5%
Total	1.1%

TABLE 2. Compton Polarimeter Systematic Errors

Laser Polarization	0.7 %
Gain Shift	0.9%
Collimator Position	0.02%
Nonlinearity	0.3%
Total	1.2%

liters per hour on average, with peak loads of 33 lph during initial colddown. For smoother operation with less downtime, we should upgrade and automate the cryogenic system for the high-field magnet. The upgrade has been designed and is straightforward. It has been estimated to cost 250K$. This infrastructure upgrade will be of general use, e.g. it is needed for the 12 GeV MOLLER experiment.

2   Compton Polarimeter

The Compton polarimeter was upgraded prior to the PREX-I run to achieve an improved figure of merit at low energies by using a new green laser and a new resonant cavity and refurbished optics table. The signals from back-scattered photons were integrated in custom Flash ADCs. This integration technique eliminated the systematic error from thresholds that affected the older counting method, as well as eliminated the deadtime. What's more, the exclusive reliance on the integration technique allowed us to handle significantly more background than in previous running (HAPPEX-III and PVDIS), and hence we were not as sensitive about the beam tuning in the Compton apparatus. Indeed, the Compton results were very clean, see fig 4 for the asymmetry versus time during PREX-I. Table 2 shows the systematic errors achieved during PREX-I which totaled 1.2%, a major accomplishment for 1 GeV running.

E   Statistical Noise

To obtain the necessary statistical precision, our cumulative pulse-pair width (in 30 msec) had to be $\ll$ 200 ppm. During the running at 70μA we observed a width of 171 ppm in the measured asymmetry (fig 1). To achieve the necessary electronic noise requirement, custom 18-bit ADCs were built by the JLab electronics group. In addition, running at a higher rate of helicity flipping helped. We had the option to run at 240 Hz, but found 120 Hz more convenient. To achieve a narrow width from the integrating detector for 1 GeV, new quartz detectors were developed by UMass and Smith College.

F   Lead Target

A major concern was developing a Pb target that could operate at high beam currents without melting. We successfully accomplished this to beam currents exceeding 70 μA; however, we did observe two problems: 1) After about a day of running, the thickness of the target becomes non-uniform, resulting in unacceptable degradation of our pulse-pair width and thus our instantaneous statistical precision due to use of a raster. 2) After about 1 week of beam-on-target the targets might fail (but not all of them did), i.e. a hole develops and the lead melts. We believe we can succeed at running the experiment with this target design, but since we are often asked questions about these problems, a detailed explanation is warranted.

The solution to problem 1) was found during the run. We took over the raster electronics and developed a precision lock for the raster which completely eliminated the noise. The lock ensures that the raster executes the same orbit between two helicity cycles, cancelling when one takes the difference. Fig 5 shows the correlation of pulse-pair asymmetries measured on the two HRS detector systems. Since the two HRS should see different electrons, these asymmetries should be uncorrelated. The extra correlation is a sign of a common-mode noise, which would increase the running time required of the experiment. The successful cancellation of noise when we locked the raster is demonstrated in this figure.

There is reasonable evidence, both from the PREX-I run and from four test runs prior to PREX-I, that the lead target has a lifetime of order one week. After $\sim$1 week, the targets may fail suddenly. Over the history of lead target testing at JLab, 3 lead targets have failed out of 8, though not all the targets saw $\geq$ 1 week of beam. The test runs prior to PREX-I included two few-hour tests that went as high as 100μA without failure and two longer (few day) runs for the experiment e06007 which used this target design for its lead

measurements at $40 - 80\mu A$. Thermal calculations based on the numerical solution of the heat equation show that with the diamond backing the targets can withstand $\geq 100\mu A$ *if* the contact between lead and diamond is good. If there were no diamond, or no thermal contact, the lead would melt at $10 \mu A$, depending on the geometry of the rastered beam spot. We think that the main uncertainty is the thermal contact.

We believe the quality of the target construction is very important for ensuring a good contact and good heat conduction: 1) a thin ($\sim 25\mu m$) layer of "Apiezon L vacuum grease" (a pure hydrocarbon with high thermal conductivity) is applied to the lead/diamond interface. It adds negligibly to the carbon background subtraction error; 2) Belleville ("spring-like") washers used in the clamping assembly maintain a force to squeeze the lead and diamond during its thermal cycling; and 3) A silver-based paste compound used for heat-sinking in the semi-conductor industry is applied between the diamond and the copper (but is not in the central area where the beam impacts the target).

The target performance from the PREX-I run is shown in fig 6 which shows the measured rates for each target as a function of calendar time. We had three lead targets. The target with the thinnest diamond (4.5% background) degraded the fastest. Two of the targets failed, and the last target, which had the thickest diamond (8 % background) did not fail and survived the last four days of the run at $70\mu A$ with high running efficiency. Thus, there is some evidence that the thicker diamond targets are more robust. An 8 - 10% diamond background would not be a problem for the background subtraction systematic. The stability of the target is corroborated by the RMS in detector asymmetry which in the absence of other noise sources would vary as $\frac{1}{\sqrt{N}}$ for N integrated electrons in a helicity period, see fig 7. The PREX-I target experience suggests that we should run with thicker diamond and prepare enough targets (about 10) to run 25 days at high current. Since we do not need cryotarget loops on the target assembly, there is plenty of room to install $\sim$15 of these 1-inch square target foils on a linear array and move from one target to another, as is the standard procedure.

A hypothesis about the cause of the sudden failure is that either the vacuum grease or the diamond crystal structure changes in the radiation and loses its good thermal conductivity. When the conductivity goes below a critical value the lead melts. With different structures of carbon, one may obtain orders-of-magnitude different thermal conductivities. These range from diamond (which has the highest thermal conductivity of any solid at room temperature) to a form of graphite that is used commercially to insulate furnaces. The effective lifetime of the Apiezon vacuum grease is of order 100 MRad [34]. For CVD diamond the lifetime has been studied [35] by measuring "thermally stimulated current" which provides information on the energy levels and impurities

in the lattice, which we suppose would be related to changes in thermal conductivity. The studies were done for detectors in a high radiation environment and find a lifetime exceeding 1000 MRad (10 MGy) for 10 keV to MeV range photons. Since no degradation was found, we assume this is a lower bound to the lifetime of the diamond. The authors concluded that diamond is one of the more attractive materials for withstanding high radiation for their application. Based on an energy deposition of $\sim 2 \frac{\text{MeV}}{\text{g/cm}^3}$ we estimate the dose rate in diamond is $\sim 7 \times 10^4$ MRad/hr for 100 μA of beam, which of course gives a much higher dose in 1 week than the lifetime bound that we found in the literature.

Radcon safety experience from the target failures of PREX-I is also relevant. When the target fails, the vacuum chamber becomes contaminated with a very thin layer of Pb that plates out on cold surfaces. Each Pb target is in 1/2 inch deep re-entrant copper wells and are somewhat isolated from each other. We should not need to access the target chamber during the experiment. After PREX-I finished, the target group had to wait several days for radiation levels to subside before removing the target and cleaning the chamber. The cleanup was a routine operation.

Some observers have suggested a spinning target design or other design modifications to improve the thermal performance. A potential problem with the spinning design is that it might introduce 100 ppm level noise, the way the raster did. We have already learned how to eliminate this noise for a fixed target by synching the raster, see the discussion above. Initial synching with 1 μsec time jitter was not sufficient; in the end, the jitter was 10 nsec and was sufficient. It would be difficult to synch a spinning target at the required level. Dave Meekins of the target group has suggested that to improve the thermal contact between lead and diamond we can either sputter lead onto diamond, or diamond onto lead. The former would probably be easier. There is a setup in the JLab target group to try this and they are willing to support us.

The collaboration feels that it has a well-tested, working target, albeit with a 1 week lifetime, and there is some evidence that thicker diamond backing improves the robustness. This should be sufficient to finish the lead measurements.

We are willing to try two simple alternative designs that have been suggested : 1) using rigid graphite (another form of carbon) as a backing; and 2) using multiple layers of thinner diamond and lead to potentially improve the thermal contact. It would be easy to commission these targets at the start of the next run since many targets can be fit inside the scattering chamber. The rigid graphite was suggested by Dave Meekins. From the extensive experience of the target group at JLab, these rigid graphite foil targets are known to be

extremely robust. For example, they can withstand $100\mu A$ of beam with no raster. However, their thermal conductivity is smaller than diamond, though still higher than Pb. Thermal calculations show that a Pb/graphite sandwich cannot run at beam currents higher than $60\mu A$ for a 4 x 4 mm raster.

In conclusion, we propose to use 10 Pb/diamond targets, as well as 2 Pb/graphite targets and 2 multiple-layer targets for PREX-II. The new target designs could be tested during the early phase of the experiment.

IV   REMAINING TECHNICAL ISSUES

A   Vacuum Seals

A primary source of downtime during PREX-I was the failure of a soft O-Ring that was part of the vacuum coupling of the scattering chamber to the exit beam pipe. We will need to redesign this section so that the seals are all-metal, for example conflat flanges. The challenge is not only radiation hardness but also durability due to significant thermal cycling.

B   Radiation Load and Septum Modifications

Although the radiation at the site boundary was not a problem for PREX, the radiation inside the hall caused significant failure of the controls systems and loss of running efficiency. The beamline downstream of the scattering chamber must be designed to mitigate the large radiation dose. The main goal is to reduce the radiation deposited in the hall by a factor of ≥ 10 compared to PREX-I, which we believe would make the experiment run like an "ordinary" Hall A experiment. A second goal is to make the Hall A instrumentation more radiation-hard, which is a goal already being pursued by the technical staff. For example we have already replaced the valve controllers so that they are more robust, and efforts are underway to replace critical electronic boards with more radiation-hard designs.

The main source of damaging radiation is neutrons resulting from the interaction of elastically scattered electrons from the lead target with materials downstream. The neutrons result from photonuclear reactions. The elastic lead cross section is large (due to Z^2) and these electrons carry most of the energy of the beam. The beam pipe leading to the beam dump restricts the maximum scattering angle to be $\theta \leq 0.95°$, and we cannot open that up because the spectrometers are very close to the beamline. During PREX-I, a

tungsten (W) collimator absorbed 1 kWatt from the range $1.1° < \theta < 3°$. Beyond $3°$ the power drops to less than 5%, so the main problem is to absorb safely the range $0.95° < \theta < 3°$.

During PREX-I, the W itself was not shielded and became a major source of neutrons from photonuclear reactions. Most of these neutrons have energy lower than a few MeV. The radiation damage for electronics is caused by elastic scattering of 0.1 to 10 MeV neutrons from nuclei, see the damage curve for silicon (fig 8 and [36]). Measurements with detectors that can distinguish neutrons from gammas and also detect thermal neutrons will be taken to verify this. The damage to electronic equipment from thermal neutrons is much smaller. The cross section for elastic scattering from H, which greatly reduces the energy of the neutrons, is 20 barns at thermal energy and decreases to a few barns at the MeV level. Thus 20 cm of polyethylene is sufficient to degrade the energy of our neutrons so that they are no longer a source of radiation damage. Since the neutron cross section rises with decreasing energy, the neutron entering polyethylene penetrates a reasonable distance, loses energy so that the cross section is large, and can no longer escape. Hence few-MeV neutrons in polyethylene tend to behave more like showering electrons in Pb or W and not like atoms in a gas.

The problem of reducing the neutron radiation is challenging because

- Shielding neutrons usually takes at least 0.5-1 m of concrete or polycrete. There are space and weight problems with this amount of material.

- Neutrons do a lot of elastic scattering, so that they are closer to a gas than a flux of particles. Consequently, many of the neutrons might exit holes in the shielding, reducing the effectiveness of the shielding. For the PREX geometry, it is hard to eliminate the holes.

There are two options we are considering for mitigating the radiation:

- Put a new tungsten collimator right after the target that blocks from $0.78° < \theta < 3°$ (see fig 9). This collimator will need to be water-cooled and shielded with $\geq$20 cm of polyethylene. Alternatively we are considering poly-concrete and borated-concrete (see below). Preliminary simulation results for the neutron flux relative to a benchmark of LD2 running are shown in fig 11.

- Put a set of collimators at locations both near and further away from the target. One would be near the gate valve ($1.3°$ restriction) and another near the primary restriction ($0.95°$ restriction) of the corrugated exit beam pipe. These would also likely be made of tungsten and shielded with the aforementioned concrete materials.

17

Neutrons are also produced in the target (fig 10) but they are fewer than from the tungsten collimator because less power is deposited in the target. Fig 10 shows a comparison of the Geant3/DINREG [37] code to Geant4 and FLUKA for the lead target alone. We are doing this for various target thicknesses. The good agreement shows that we are well on our way towards simulating the radiation reliably. We remind the reader that the thickness is 10% of a radiation length and was optimized for the original proposal to solve the following problem: for an energy bite defined by our detector necessary to discriminate inelastic levels we want to maximize the rate. As the target thickness grows, the radiative losses push more scattered electrons outside this bite.

We are considering using the special concrete materials invented at JLab for the SHMS shield hut in Hall C [38]. The "polyethylene-concrete" consists of polyethylene plastic embedded in a concrete mixture. The "borated-concrete" used for SHMS is a new material consisting of boron carbide, Portland cement, and water, i.e. the boron carbide is the "sand" of the concrete mix. The borated-concrete is 55% elemental boron. Both of these concrete mixtures are structurally strong and can be formed into shapes and have high melting temperatures. The poly-concrete tends to slow the neutrons, while the borated-concrete absorbs them.

To provide space for possible shielding after the Q1 quads we are considering opening up the HRS spectrometer angle to 13.5° (PREX-I ran at 12.5°). However, if the shielding strategy mentioned in the first option listed above is sufficient this opening would not be necessary. Opening to 13.5° would require running the septum magnet with a higher field (1.2 T-m) by adding a third coil and using a second power supply. In addition we would open up the central bore of the septum to provide more space on the beamline. Adding the third coil would, however, reduce our solid angle by $\sim$15% and degrade the hardware resolution. Preliminary estimates (see fig 12) show that this compromise is acceptable.

An initial simulation of the neutron radiation load from the PREX setup has been performed with Geant-4. We have also checked these computations with a FLUKA code. The simulations consider the source term near the target and collimator (see fig 11). The W collimator with an opening angle of 0.78° was used. The simulations show a significant reduction of the radiation in the hall. The work is in progress and the materials and their geometric arrangement need to be optimized to be able to reach our goal. The shielding configuration shown fills the available space between the scattering chamber and the septum water attachments with borated polyethylene (see figure 9). Simulations show that the specialized concrete materials mentioned above also reduce the neutron flux in the hall.

18

Some further practical considerations

- The polyethylene might overheat or crumble due to radiation. It can be encased in aluminum to avoid this problem. Water is another possibility, but water leaks would be a concern.

- To reduce holes from which neutrons can leak, polyethylene in aluminum can be put in the incoming beam line. In addition, there may be room in the septum magnet gap or downstream of the septum to add polyethylene. A detailed full-scale monte carlo study will need to be done of the entire setup. This will hopefully show, for example, that neutrons entering the iron of the septum will diffuse to the polyethylene and lose their energy there until they are harmless to electronics.

In summary, we believe we can reduce radiation load in the hall to an acceptable level to avoid failure of electronic equipment. More simulation effort and beam tests will be done to prove this before we run.

V   PROPOSED RUNNING STRATEGY

Using the optimal setting of the septum magnet and a slightly lower energy we can project the accuracy of a future run. In figure 13 we show how the rate varies with the septum current and Q^2. The optimum kinematics is one that minimizes the error in R_N. The result of this optimization procedure is shown in fig 14. Fig 15 shows how this proposal would compare to the PREX-I result and to various models. Note that both the asymmetry and the sensitivity to R_N grows with Q^2, and the rates drop with Q^2. In order to minimize systematic errors due to these three factors, we want to run at the higher end of the optimal Q^2 range. For a 30 total days of running, the total error in R_N will be 1 % if a beam polarimetry error of 1% is achieved. Considering that we already have 5 PAC days of good data, we are requesting 25 more PAC days to complete the experiment.

Table 3 shows the rates, asymmetries, and running time for the PREX-II proposal.

In the following, we briefly discuss how PREX-II could fit into the 12 GeV era. Since Hall A's upgrade plans are simpler (no major new installations), the default plan has it being the first hall ready for beam. As a "DOE deliverable", the first physics research is expected to occur in FY15 (starting Oct 2014), and there are several proposed or approved Hall A 12 GeV experiments that require little or no new equipment other than the beam itself. However,

during the time frame of late 2013 to Fall 2014 (FY14) when 12 GeV beam commissioning is well under way, Hall A will be the beam delivery point for pre-operational tests and engineering runs. Although there are no formal plans to provide research-quality beam to Hall A, we propose to be ready to receive beam if the accelerator commissioning goes well. The collaboration has had close communications with the Electron Gun Group as well as Accelerator Operations to achieve beam delivery specifications for the previous measurements. We expect to continue this successful collaboration during PREX-II and lay the foundation for the future 12 GeV parity experiments MOLLER and SOLID.

We address two aspects of the technical challenges of PREX-II that might be of concern. The first involves "parity quality" in terms of reduction of helicity correlations in the electron beam. With the additional successful operation of the "Double Wien" filter, the specifications achieved for PREX-I will be adequate to carry out PREX-II. It is worth noting that the polarized source is not scheduled to be upgraded until FY15, so all of the experience gained to date will be directly applicable should PREX-II be scheduled during FY14. The second issue involves the beam quality required for successful operation of the Compton polarimeter. With the successful operation of the green laser and the technique of integrating the back-scattered photon signal during PREX-I, we found that we could handle significantly more background than in previous runs (HAPPEX-III and PVDIS). We are therefore quite optimistic that beam delivery will be of high efficiency and high quality despite the changes induced by the accelerator upgrade.

During the FY14 commissioning, the Hall D beam will also be commissioned. Since this is a new hall and an entirely new beam configuration, frequent accesses might be required. The PREX commissioning plan as well as production running configuration is very flexible and the collaboration is keen to work with the accelerator division to be ready to take beam over an extended period where frequent switches to beam delivery is made between Hall A and Hall D. Once the experiment is commissioned, production running can be established within a matter of a few hours each time. Given the technical challenges of the experiment, PREX-II will also profit from breaks that might be built into the schedule in this scenario.

VI   COLLABORATION STATUS

We have added Kent Paschke as a co-spokesperson. The experiment is a Hall A collaboration proposal, and the core experimental group is the HAPPEX collaboration which has completed six parity experiments in Hall A since 1998

TABLE 3. PREX-II Proposed Data

Measured Asymmetry ($p_e \ A$)	0.51 ppm
Beam Energy	925 to 1000 MeV
Beam Current	$70\mu A$
Statistical Accuracy (combine with PREX-I)	3%
Detected Rate (each spectrometer)	740 MHz
PREX-II Production	25 days
Setup, Calibrations, Møller	10 days
Total Time Request	35 days

[39]. In addition, several collaborators were central to the the SLAC parity experiment E158 [40] and several others are members of the Qweak collaboration.

VII   COMMENTS ON OTHER FUTURE PLANS

There is an interest in performing parity-violating measurements from other nuclei; the consensus on the candidates for a next series of runs are ^{48}Ca, ^{40}Ca, and isotopes of tin: ^{112}Sn, ^{120}Sn, and ^{124}Sn, see ref [41]. Statistical errors better than 1% appear to be feasible with 30 day runs. The ^{48}Ca measurement is optimized at a beam energy of ~ 2 GeV, making it an ideal 1-pass experiment for Hall A in the 12 GeV era. However, the collaboration would like to complete the running on ^{208}Pb first. The reasons to use ^{208}Pb remain the same as originally proposed: 1) Lead is a very well-known nucleus and has a simple structure (doubly-magic); 2) It has the highest separation to the first excited state (2.6 MeV) of any heavy nucleus. Combined with the high momentum resolution of our spectrometers, this separation lends itself well to the flux integration detection technique; 3) ^{208}Pb is thought to have a relatively large value of R_N. 4) Since ^{208}Pb is a heavy nucleus, with a large number of extra neutrons, there should be a relatively clean interpretation of the skin thickness in terms of properties of bulk neutron matter.

VIII   BEAM TIME REQUEST

We request 35 days of polarized beam running in Hall A at 925 to 1000 MeV using the 5° degree septum magnets. This includes 5 days of commissioning and 5 days of overhead for Møller Polarimetry and auxiliary measurements.

REFERENCES

1. B. Frois et al., Phys. Rev. Lett. **38**, 152 (1977).
2. C. Garcia-Recio, J. Nieves and E. Oset, Nucl. Phys. A **547**, 473 (1992).
3. L. Ray, W. R. Coker, G. W. Hoffmann, Phys. Rev. C **18**, 2641 (1978).
4. V. E. Starodubsky, N. M. Hintz, Phys. Rev. C **49**, 2118 (1994).
5. B. C. Clark, L. J. Kerr, S. Hama, Phys. Rev. C **67**, 054605 (2003).
6. A. Trzcinska et al., Phys. Rev. Lett. **87** , 082501 (2001).
7. H. Lenske, Hyperfine Interact. **194**, 277 (2009).
8. T. W. Donnelly, J. Dubach, Ingo Sick, Nucl. Phys. **A503**, 589 (1989).
9. C. J. Horowitz, Phys. Rev. C **57** , 3430 (1998).
10. C. J. Horowitz, S. J. Pollock, P. A. Souder, R. Michaels, Phys. Rev. C **63**, 025501 (2001).
11. Y. Shin et al., Phys. Rev. Lett. **97**, 030401 (2006).
12. G.B. Partridge et al., Science **311**, 503 (2006).
13. B. A. Brown, Phys Rev. Lett. **85**, 5296 (2000).
14. K. Hebeler, J.M. Lattimer, C.J. Pethick, A. Schwenk, arXiv:1007.1746.
15. S. Gandolfi, J. Carlson, Sanjay Reddy, arXiv:1101.1921.
16. C. J. Horowitz, J. Piekarewicz, Phys. Rev. **C64**, 062802 (2001).
17. Feryal Ozel, Gordon Baym, Tolga Guver, arXiv:1002.3153.
18. Andrew Steiner, James M. Lattimer, Edward F. Brown, arXiv:1005.0811.
19. Feryal Ozel, Gordon Baym, Tolga Guver, Phys. Rev. D **82**, 101301 (2010).
20. W. G. Lynch, M. B. Tsang, Y. Zhang, P. Danielewicz, M. Famiano, Z. Li, A. W. Steiner ArXiv:0901.0412.
21. M.B.Tsang, Yingxun Zhang, P.Danielewicz, M.Famiano, Zhuxia Li, W.G.Lynch, A.W.Steiner, Phys. Rev. Lett. **102**, 122701 (2009).
22. C.J. Horowitz, J. Piekarewicz, Phys. Rev. **C66**, 055803 (2002).
23. C. J. Horowitz, J. Piekarewicz, Phys. Rev. Lett. **86**, 5647 (2001).
24. S. J. Pollock, E. N. Fortson, L. Wilets, Phys. Rev. C **46**, 2587 (1992).
25. B. A. Brown, A. Derevianko, V. V. Flambaum, Phys. Rev. C **79**, 035501 (2009).
26. K. Tsigutkin, D. Dounas-Frazer, A. Family, J. E. Stalnaker, V. V. Yashchuk, D. Budker, arXiv:1001.0587.
27. G. A. Lalazissis, J. Konig, and P. Ring, Phys. Rev. C55, 540 (1997).
28. B.G. Todd-Rutel, J. Piekarewicz, Phys. Rev. Lett. 95, 122501 (2005).
29. C.J. Horowitz, private communication.
30. M. Beiner, H. Flocard, N. Van Giai, P. Quentin, Nucl. Phys. A 238, 29 (1975).
31. E. Chabanat, P. Bonche, P. Haensel, J. Meyer, R. Scha- er, Nucl. Phys. A 635, 231 (1998).
32. D. Vautherin, D. M. Brink, Phys. Rev. C 5, 626 (1972).
33. M. Hauger *et al*, Nucl. Instr. and Methods A 462 (2001) 382.
34. Data sheets on http://www.apiezon.com/apiezon-l-grease.htm
35. T. Behnke, *et. al.* NIM A489 (2002) 230.
36. P. Degtiarenko, A. Fasso, G. Kharashvili, A. Somov, JLAB-TN-00-000 (GlueX-doc-1660) P.J. Griffin et al., SAND92-0094 (Sandia Natl. Lab.93) 1996; A. Konobeyev, J. Nucl. Mater. 186 (1992); M. Huhtinen and P.A. Aarnio, NIM

A 335 (1993) 580; G.P. Summers et al., IEEE NS40 (1993) 1372.

37. Geant3/DINREG Radiation Simulation Code, Pavel Degtiarenko, JLab Radiation Control Group.

38. P. Brindza and T. Horn, private communications.

39. K. A. Aniol *et al.*, Phys. Rev. Lett. **82** 1096 (1999). K. A. Aniol, *et al.*, Phys. Rev. C 69, 065501 (2004). K. A. Aniol, *et al.*, Phys.Rev.Lett.96:022003,2006. K. A. Aniol, *et al.*, Phys.Rev.Lett.98:032301,2007.

40. P.L Anthony, *et.al.* Phys.Rev.Lett.95:081601,2005.

41. Shufang Ban, C. J. Horowitz, R. Michaels, arXiv:1010.3246
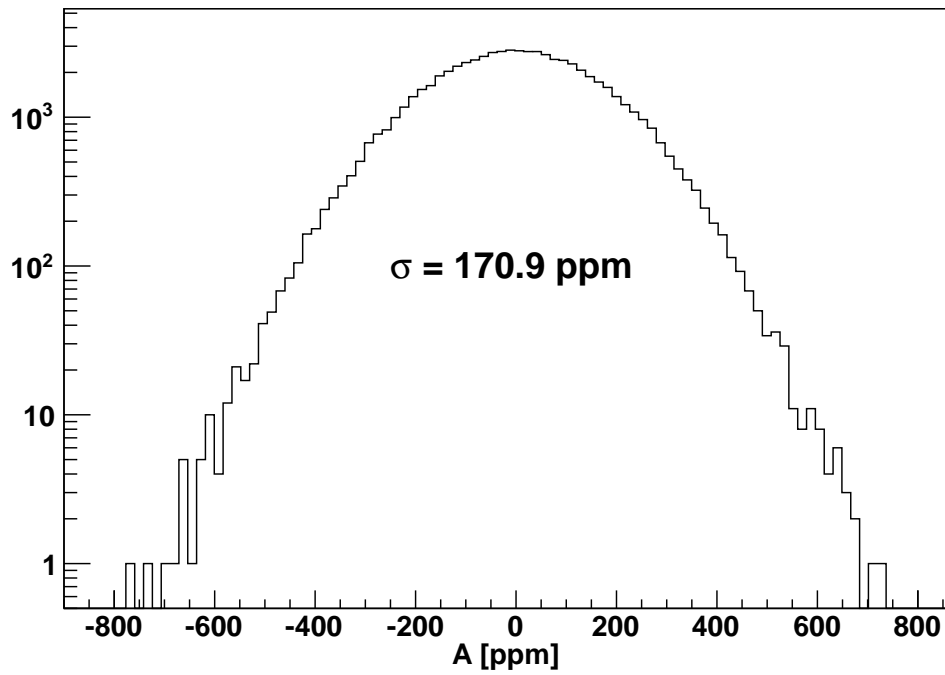
FIGURE 1. Distribution of the asymmetries for a typical run at 70μA. Beam-related noise has been subtracted using the standard "dither correction" method. The width of 171 ppm is consistent with counting statistics.
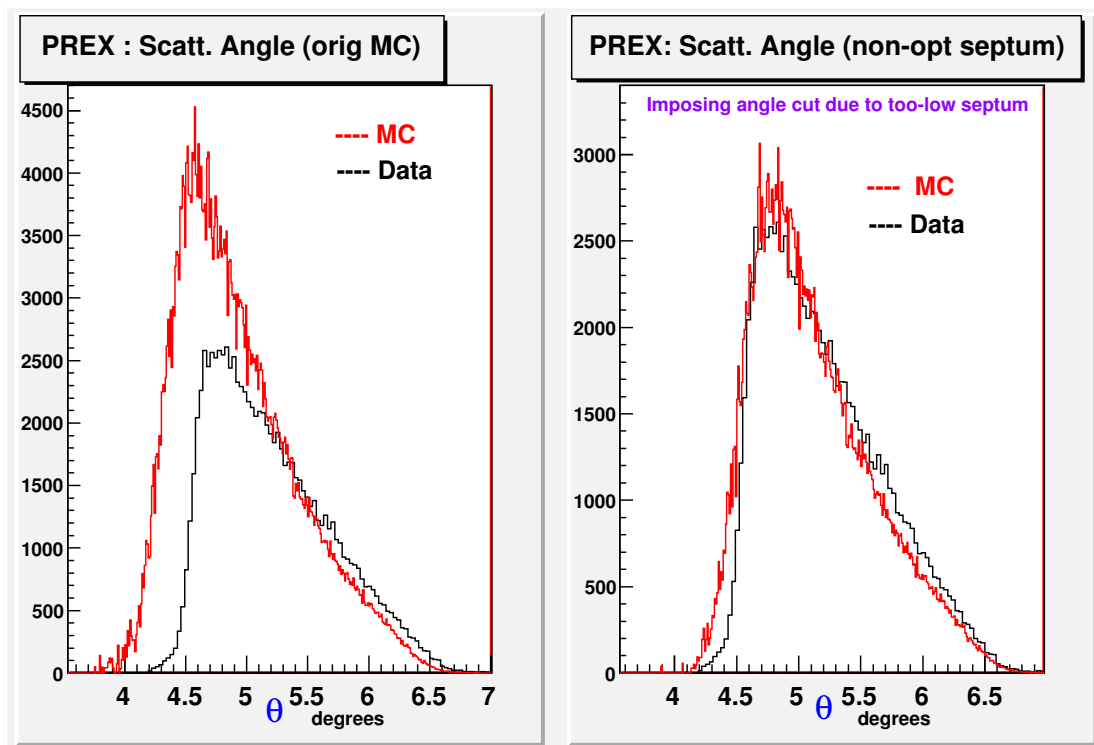
FIGURE 2. Simulated and reconstructed scattering angle. The data are compared to the original simulation (left) and a corrected simulation (on the right), where the correction takes into account that the septum current was set too low by 5% such that the scattering angle cutoff was too high by 5 mrad (0.3°).

25
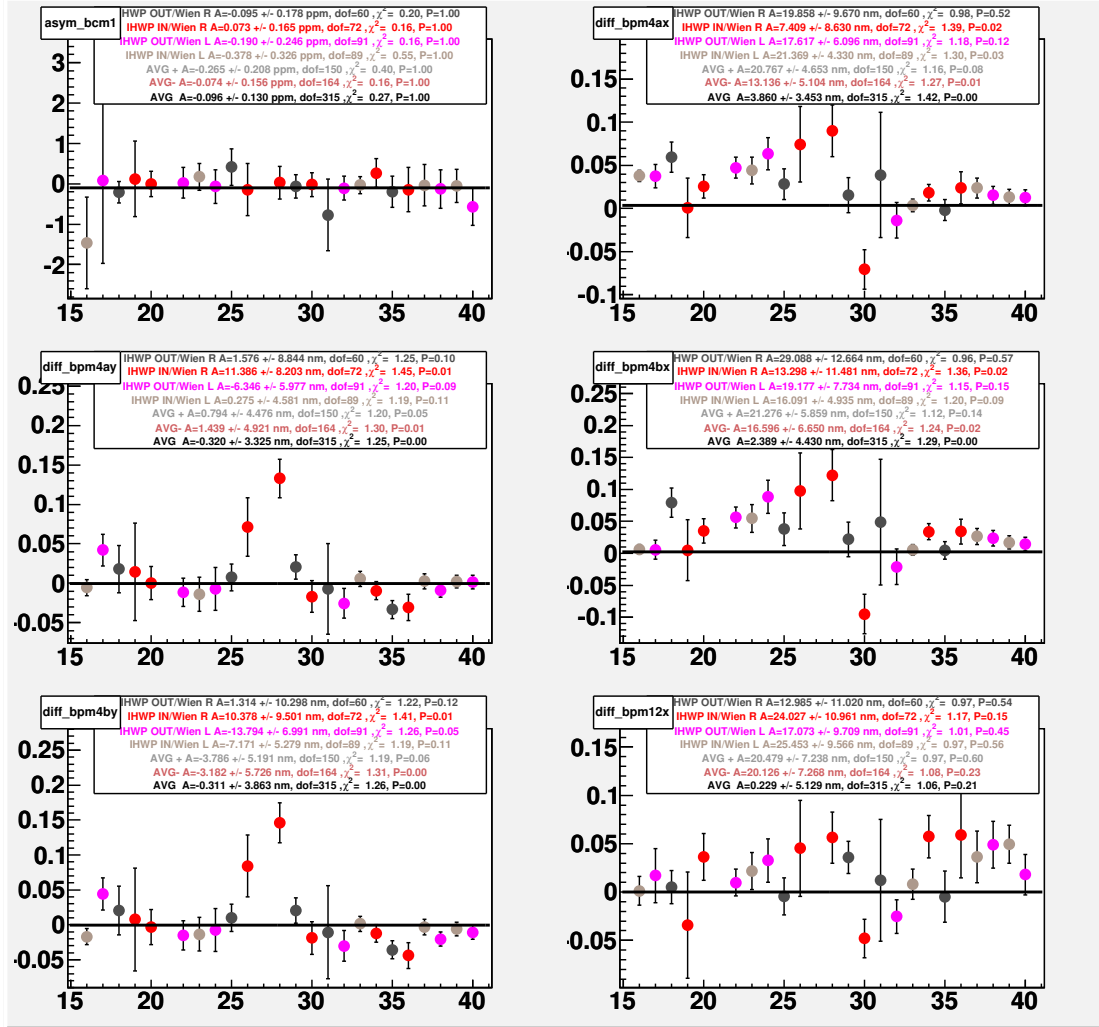
FIGURE 3. Helicity-correlated charge asymmetries and position differences versus slug (a slug is ~ 1 day of running). To illustrate the systematics, the data points are plotted without sign correction for the helicity flip. The final average with all sign corrections is shown by the black horizontal bar and was controlled at the 5 nm level averaged over the PREX-I run. The charge asymmetry was forced to zero by the standard feedback system.

26
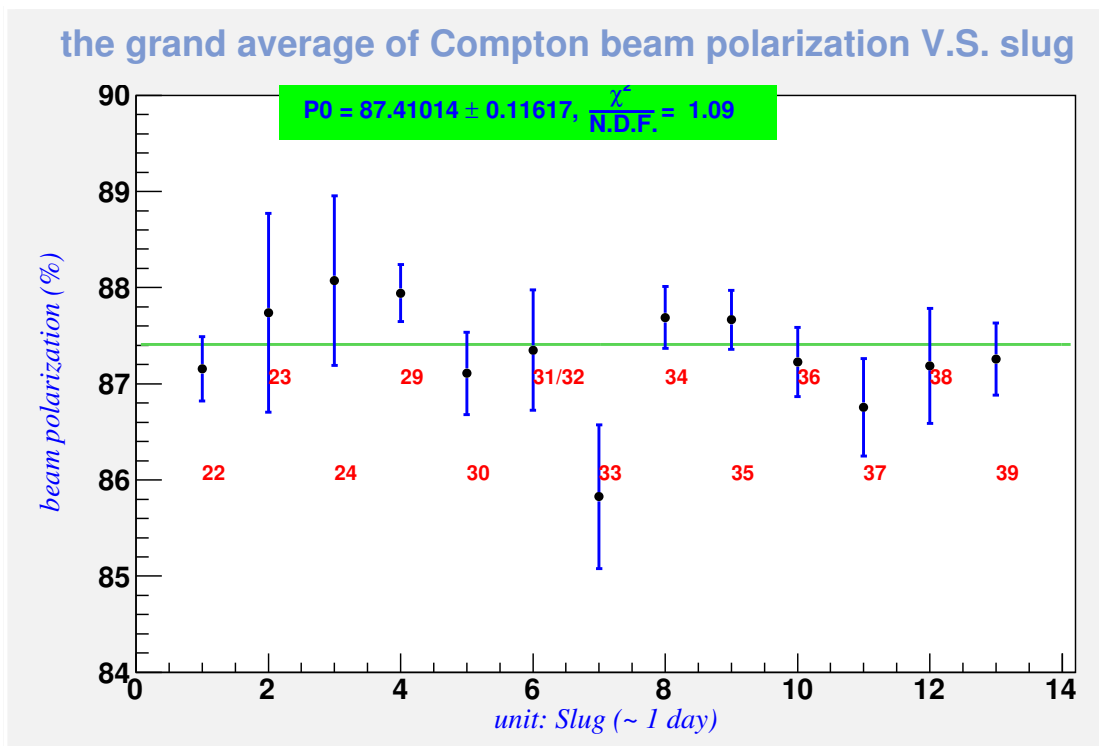
FIGURE 4. Slug plot of the Compton beam polarizations during PREX-I. A systematic error of 1.2% was achieved.
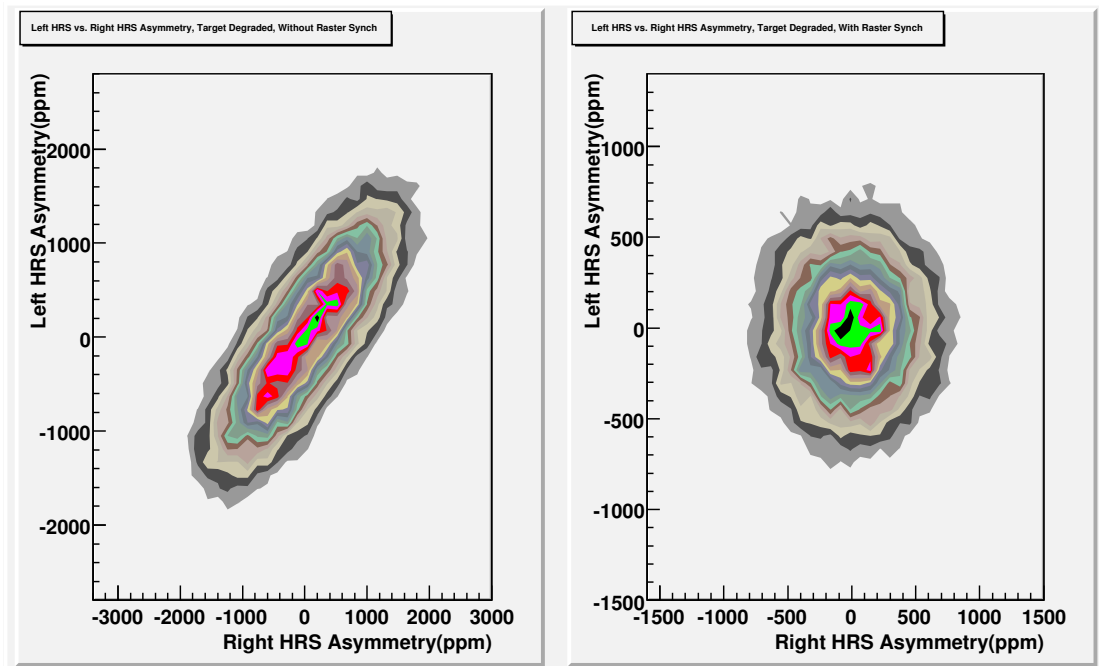
FIGURE 5. Correlation of the pulse-pair asymmetry between left and right HRS detectors. A common source of noise leads to a correlation. On the left we show the data when the the target had degraded. On the right we show the recovered performance when we synched the raster to the helicity flip rate. The data before target degradation looked similar to this.
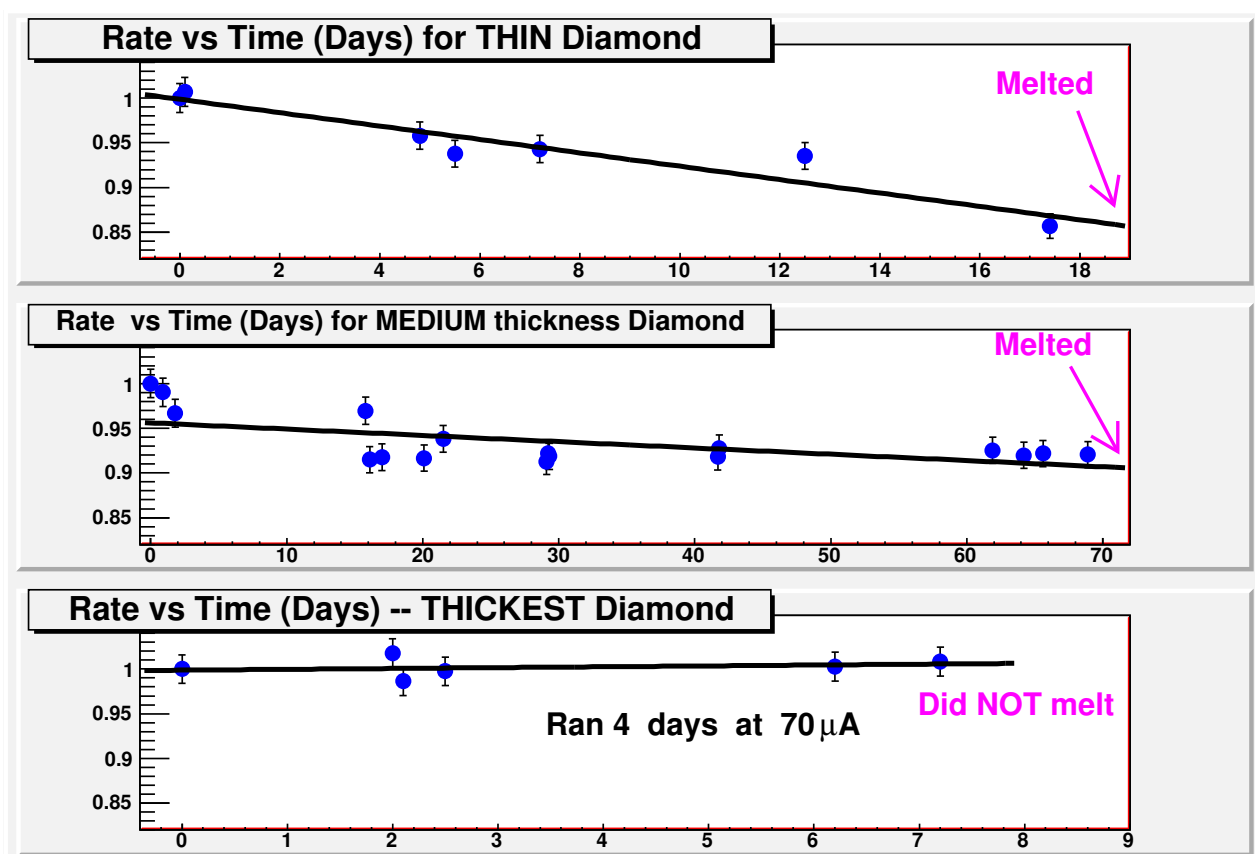
FIGURE 6. Rate measured in counting mode versus time in days for the three Pb/diamond targets. The target with the thinnest diamond backing (4.5% background) degraded the fastest. Two of the targets melted. The target with the the thickest diamond (8%) did not melt and ran for 4 days at 70μA (and 7.5 days total).
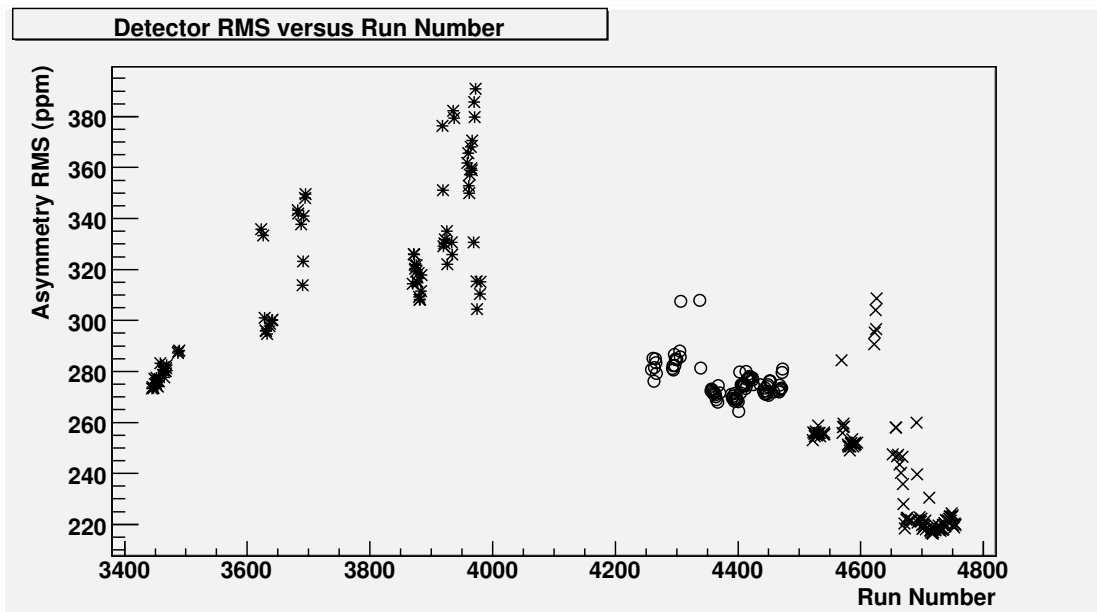
FIGURE 7. The RMS in the measured asymmetry versus run number. It is another indicator of the target integrity. Some initial large RMS are due to learning about the raster synching. From run 4660 to the end we ran with 70μA.

Displacement damage in Silicon
for neutrons, protons, pions and electrons
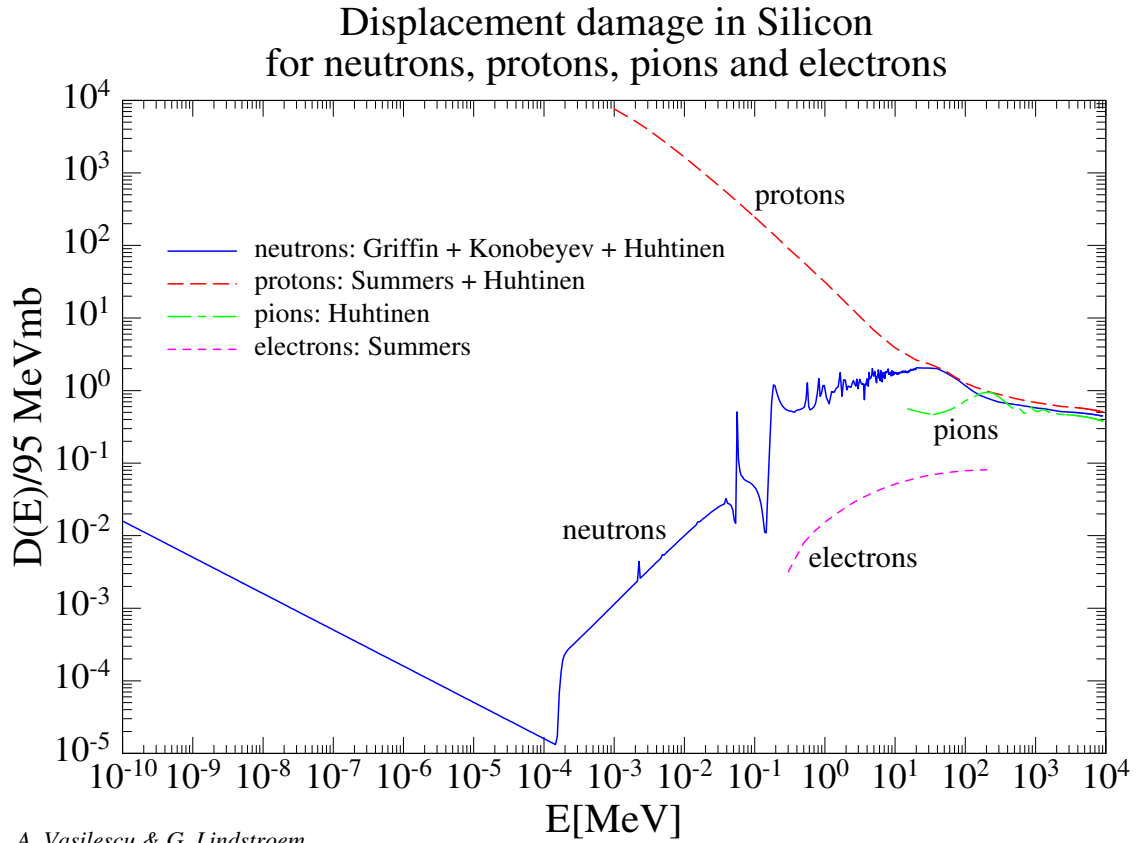
A. Vasilescu & G. Lindstroem

FIGURE 8. Silicon damage curve for neutron radiation. Plotted is the hardness factor k for different particles. This is defined for each particle as $k = D/D(1MeVn)$ where D is the displacement damage cross section and $D(1MeVn)$ is for 1 MeV neutrons. The displacement damage quantifies the radiation damage given by one particle at a particular energy (ref 36).
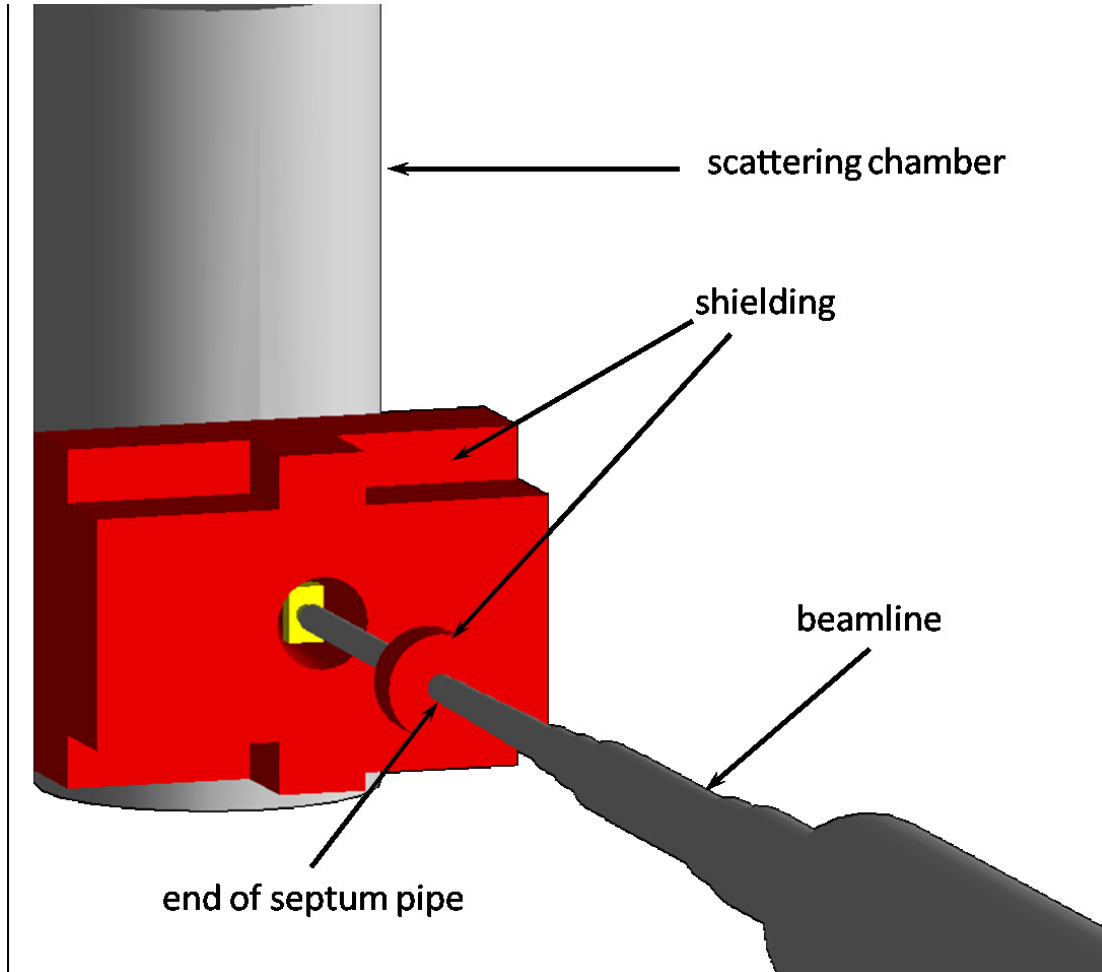
FIGURE 9. Geant4 picture of a proposed tungsten plug to absorb electromagnetic radiation in the angular range $0.78° < \theta < 3°$ surrounded by additional shielding to absorb and thermalize neutrons. The picture includes scattering chamber and stainless steel beampipe through the septum. The shielding fills the available space between the scattering chamber and the septum/attachments. The material surrounding the tungsten is borated polyethylene. The beamline is magnetically shielded and the downstream region has an acceptance $\theta < 0.95°$, so that what isn't stopped by the tungsten will transport cleanly to the beam dump.
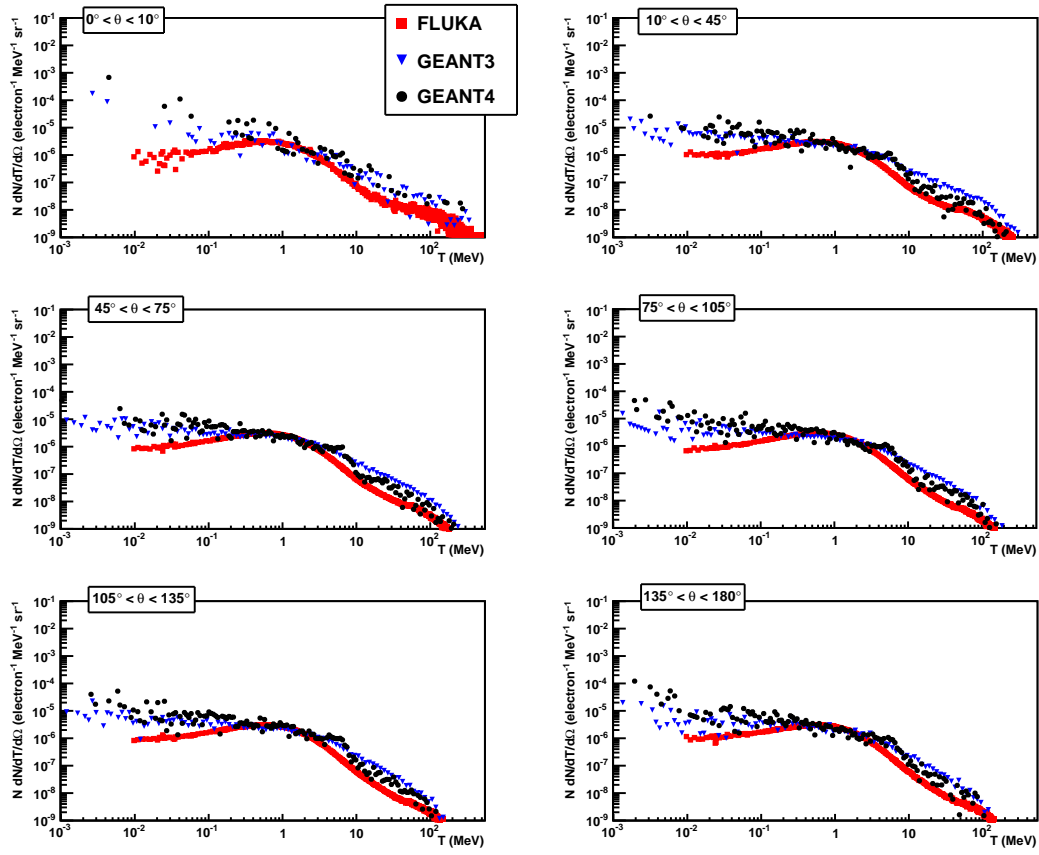
FIGURE 10. Neutron yield from a 0.5 mm lead target for three different Monte Carlo codes, Geant3/DINREG [37], Geant4, and FLUKA. The consistency is fairly good but the FLUKA yield is generally lower as its process list is less complete.
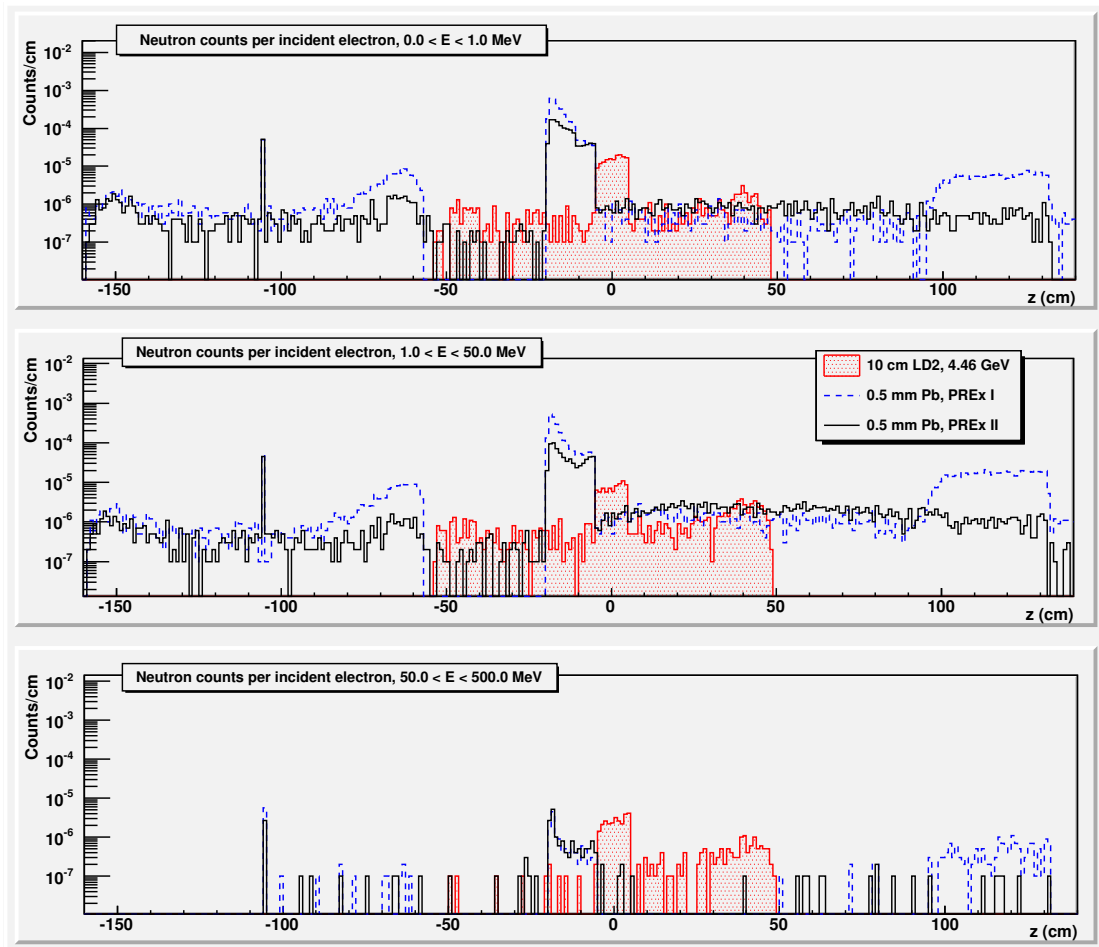
33

FIGURE 11. Monte Carlo simulation of the neutrons produced in the region around the target for each of three setups: a 10 cm LD2 target centered at z=0 cm, with a 4.46 GeV beam (SRC-like), and a 0.5 mm Pb foil at z=-105.3 cm and a tungsten collimator with a 1.09° opening angle (PREx I), and a 0.5 mm Pb target at z=-105.3 cm with a 0.78° opening angle (PREx II), both with beam energy of 1.05 GeV. In all three cases the scattering chamber is approximately centered on the target. In the PREx setups the collimator is located at approximately -20 ≤ z ≤ -5 cm and the end of the septum pipe is at approximately 120 cm. With the PREx II case there is also borated polyethylene shielding in the region between the scattering chamber and the septum magnet. The goal is to bring the radiation load down a factor of ∼ 10 from PREX-I and close the LD2 benchmark.
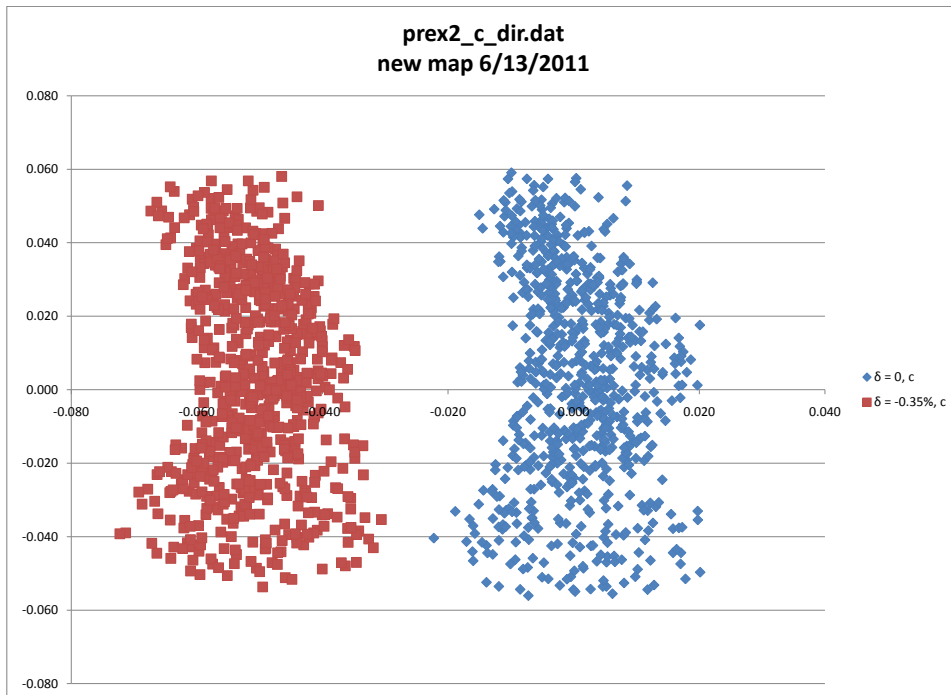
34

FIGURE 12. Hardware resolution for the modified higher-field septum to allow the option of a more open geometry (13.5° angle for HRS). Shown is the position separation of track bundles (X,Y location at the detector) for a 3.5 MeV shift in momentum. The resolution is sufficient to discriminate excited states.
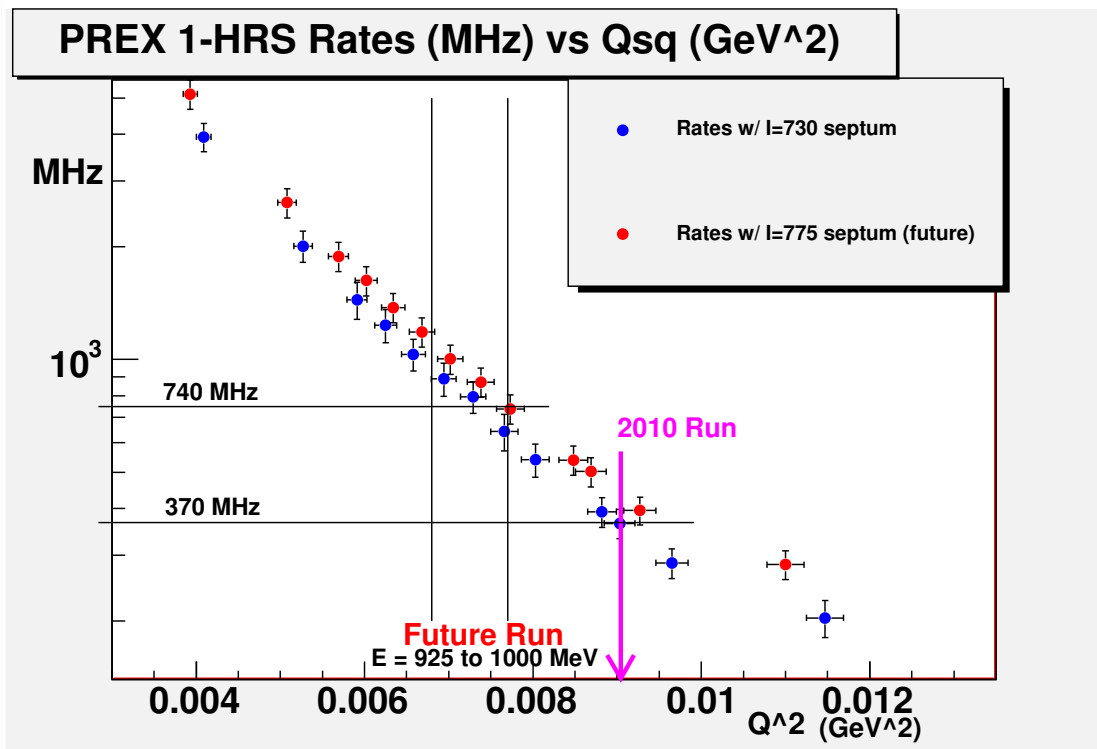
FIGURE 13. Simulated rates in one HRS versus Q^2 for two assumptions about septum current setting. For I=729 Amps (2010 run) the minimum scattering angle was 4.58 degrees and was not optimal. For I=775 Amps (suggested future run point) the min angle will be 4.35 degrees. By putting the septum there and reducing the energy to the range 925 to 1000 MeV, we expect to double the rate.
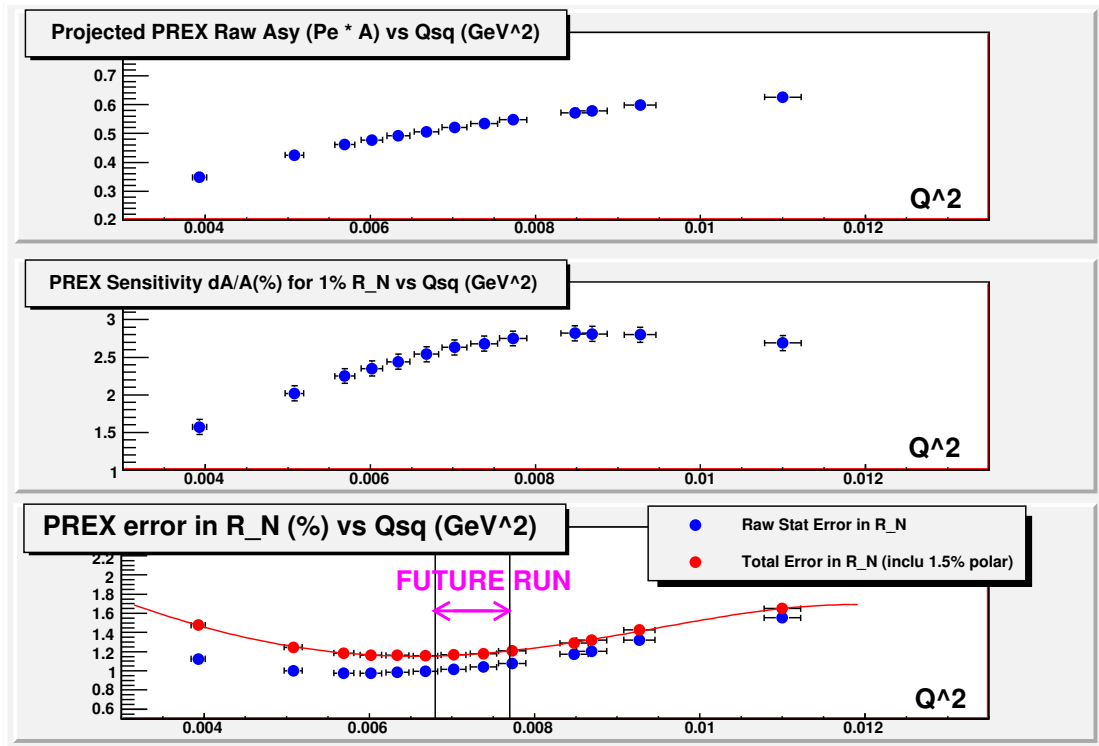
FIGURE 14. The raw asymmetry, sensitivity to R_N, and error in R_N as functions of Q^2 for the correct septum current (I=775 Amps). We'll want to run at an energy between 925 and 1000 MeV, which provides a statistical error in R_N of 1% in 25 addional days at 70μA.
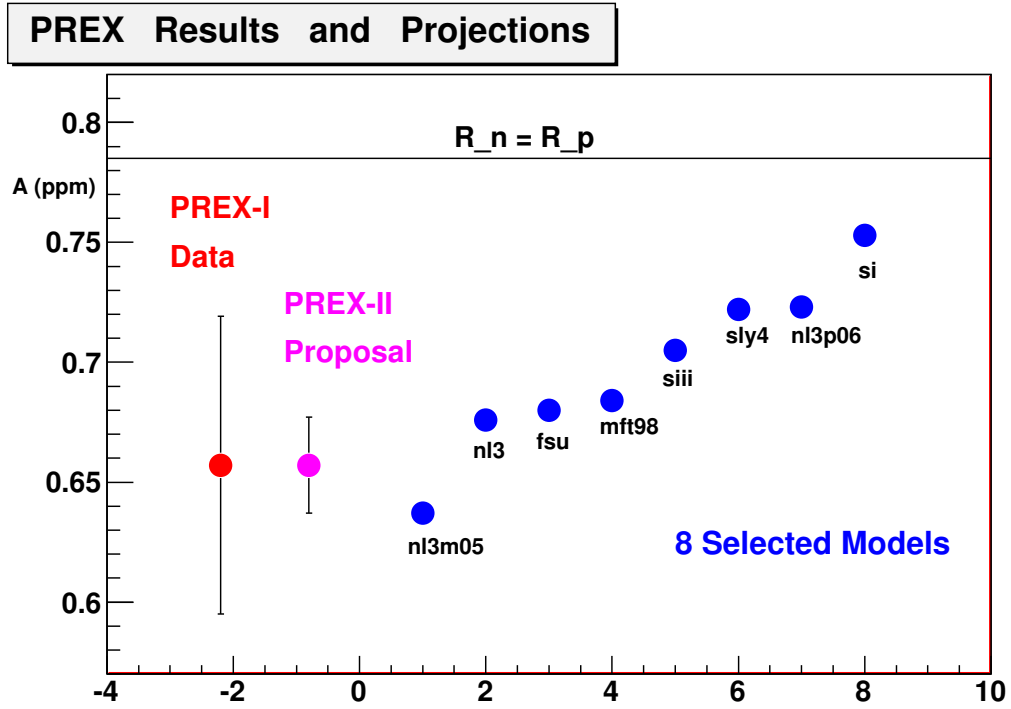
FIGURE 15. The PREX asymmetry for the PREX-I data, the PREX-II projections (present proposal), and 8 selected models. Also shown is the asymmetry for the hypothesis that the neutron radius is the same as the proton radius. References: nl3m05, nl3, and nl3p06 from [27], fsu from [28], mft98 from [29], siii from [30], sly4 from [31], si from [32].